Journal of the International Neuropsychological Society (2009), **15**, 671–683.

doi:10.1017/S1355617709990233

Molecular neurodevelopment: An *in vivo* ^{31}P-^{1}H MRSI study

GERALD GOLDSTEIN,[1] KANAGASABAI PANCHALINGAM,[2] RICHARD J. MCCLURE,[2] JEFFREY A. STANLEY,[6] VINCE D. CALHOUN,[7,8,9] GODFREY D. PEARLSON,[9] AND JAY W. PETTEGREW[2,3,4,5]

[1]VA Pittsburgh Healthcare System, Pittsburgh, Pennsylvania
[2]Department of Psychiatry, University of Pittsburgh School of Medicine, Pittsburgh, Pennsylvania
[3]Department of Neurology, University of Pittsburgh School of Medicine, Pittsburgh, Pennsylvania
[4]Department of Behavioral and Community Health Sciences, University of Pittsburgh School of Medicine, Pittsburgh, Pennsylvania
[5]Department of Bioengineering, University of Pittsburgh, Pittsburgh, Pennsylvania
[6]Departments of Psychiatry and Behavioral Neurosciences, Wayne State University School of Medicine, Detroit, Michigan
[7]The Mind Research Network, Albuquerque, New Mexico
[8]Department of Electrical and Computer Engineering, University of New Mexico, Albuquerque, New Mexico
[9]Department of Psychiatry, Yale University, Hartford, Connecticut

(RECEIVED October 20, 2008; FINAL REVISION May 12, 2009; ACCEPTED May 12, 2009)

Abstract

Synaptic development and elimination are normal neurodevelopmental processes, which if altered could contribute to various neuropsychiatric disorders. ^{31}P-^{1}H magnetic resonance spectroscopic imaging (MRSI) and structural magnetic resonance imaging (MRI) exams were conducted on 105 healthy children ages 6–18 years old to identify neuromolecular indices of synaptic development and elimination. Over the age range studied, age-related changes in high-energy phosphate (phosphocreatine), membrane phospholipid metabolism (precursors and breakdown products), and percent gray matter volume were found. These neuromolecular and structural indices of synaptic development and elimination are associated with development of several cognitive domains. Monitoring of these molecular markers is essential for devising treatment strategies for neurodevelopmental disorders. (*JINS*, 2009, *15*, 671–683.)

Keywords: Magnetic resonance spectroscopy, Phospholipid metabolism, Cognition, Phosphocreatine, Synapses, Brain, Child development, Adolescent development

INTRODUCTION

The four major stages that characterize human brain development are: (1) neuronal proliferation, (2) migration of neurons to specific sites throughout the central nervous system (CNS), (3) organization of the neuronal circuitry, and (4) myelination of the neuronal circuitry (Volpe, 1995).

The third stage of human brain development, organization of the neural circuitry, is most active from the sixth month of gestation to young adulthood. The major events associated with neuronal circuitry organization include: (1) proper alignment, orientation, and layering of cortical neurons; (2) dendritic and axonal differentiation; (3) synaptic development; (4) synaptic elimination (cell death and/or selective elimination of neuronal processes); and (5) glial proliferation and differentiation. These processes overlap with the timing of normal development of cognitive function and the onset of neurodevelopmental and psychiatric disorders such as attention deficit disorder, autism, and schizophrenia. Normal synaptic elimination occurs during early adolescence in nonhuman primates (Bourgeois & Rakic, 1993; Rakic, Bourgeois, Eckenhoff, Zecevic, & Goldman-Rakic, 1986) and humans (Huttenlocher, 1979, 1990; Huttenlocher & Dabholkar, 1997; Huttenlocher, de Courtten, Garey, & Van der Loos, 1982). Synaptic elimination in nonhuman primates is generally observed to occur synchronously in all regions (i.e., homochronous; Rakic et al., 1986), but is heterochronous in humans (Huttenlocher & Dabholkar, 1997). Normal synaptic elimination is predominantly of presumptive excitatory asymmetric junctions on dendritic spines (Smiley & Goldman-Rakic, 1993), which probably utilize amino acids, such as L-glutamate, as the neurotransmitter (Storm-Mathisen & Otterson, 1990). Perinatal insults, intrauterine disturbances, and perhaps environmental influences in childhood and adolescence can potentially result in disordered neuronal circuitry (Birch & Gussow, 1970). This study focuses on molecular and structural indices related to synaptic development and elimination and the correlation of these indices with measures of cognitive development.

Correspondence and reprint requests to: Jay W. Pettegrew, M.D., Director, Neurophysics Laboratory, RIDC Park, 260 Kappa Drive, Pittsburgh, Pennsylvania, 15238. E-mail: pettegre+@pitt.edu

^{31}P and ^{1}H magnetic resonance spectroscopic imaging (^{31}P-^{1}H MRSI) are well suited to monitor the processes of synaptic development and elimination and neuronal cell death by measuring energy dynamics (phosphocreatine [PCr]), a putative biomarker of neurons and neuronal processes (N-acetylaspartate [NAA]), and measures of membrane phospholipid metabolism, such as phospholipid building blocks (short nuclear magnetic resonance [NMR] correlation time phosphomonoesters [sPME]), and phospholipid breakdown products (short NMR correlation time phosphodiesters [sPDE]). The hypothesis tested in this study is that neuromolecular underpinnings of synaptic development and elimination will be observed by changes in ^{31}P-^{1}H MRSI observed brain metabolites of individuals ages 6–18, and will be associated with changes in percent gray matter by volume (GM) reflecting synaptic development and elimination. Specifically, we investigated in an axial brain slice, cross-sectional age differences in brain levels of PCr, sPME, sPDE, and NAA, which reflect changes in neuronal synaptic activity (PCr), neuronal numbers and integrity (NAA), turnover of membrane phospholipids (sPME and sPDE), and structural changes (GM). We hypothesized that these neurodevelopmental, metabolic, and structural changes would be associated with corresponding development of cognitive function in the domains of language, visual-spatial construction, executive function, and memory abilities. In an age difference study, one should expect to find meaningful correspondences among cognitive growth, the mentioned brain metabolite levels, and GM.

METHODS

Participants

The study was approved by the University of Pittsburgh Institutional Review Board. All subjects (and parents when appropriate) gave informed written consent to participate in the study. Personal interviews, including the subject and family, were conducted by a psychologist, and following the informed consent procedure and execution of the appropriate consent form, procedures were accomplished to assure that recruited participants were healthy, normally developing individuals who met all inclusion/exclusion criteria: These included a review of the study inclusion/exclusion criteria and completion and review of the Devereux Scale for Mental Disorders and a cognitive test battery as described later. This interview was followed by a separate interview in which magnetic resonance (MR) exclusion criteria were reviewed by an MR Center nurse or technician and by subject participation in an MR simulator. A pediatrician conducted the physical examination in an examination room at the MR Center. In addition to the report by the pediatrician, the Devereux scale, the family history-research diagnostic criteria (FH-RDC, Andreasen, Endicott, Spitzer, & Winoker, 1977) interview, and other tests from the cognitive neurodevelopmental battery were scored and reviewed with the subject and family. If all entry criteria were met, the full battery was completed, followed by the MRSI/MRI examination within one month after completion of the cognitive neurodevelopmental battery.

The sample consisted of 105 individuals ranging in age from 6 to 17. Fifty-four were females and 51 were males. The age distribution covered the neurodevelopmental stages of childhood (6–10 years), pubescence (10–12 years), and adolescence (12–18 years).

Neurocognitive Testing Procedures

A portion of the cognitive battery consisting of standardized tests with published manuals was administered using standard procedures under the supervision of a licensed psychologist in order to evaluate basic intellectual and academic abilities, and to detect behavioral abnormalities. This preliminary battery included an age appropriate version of the Wechsler Intelligence Scale (abbreviated WISC-R [Wechsler, 1974] for children; WASI [Wechsler, 1999] for adults) and the Wechsler Individual Achievement Test Screener (Wechsler, 2001) to identify individuals functioning within the average range of intellectual ability (IQ 85–119) with commensurate progress in the acquisition of basic academic skills. Testing was typically completed in less than four hours. In addition to satisfying criteria for nonsignificant variance in intellectual ability, individuals demonstrating significant Verbal IQ-Performance IQ (VIQ-PIQ) score discrepancies (greater than 15 points) were eliminated from the study owing to the potential for possible asymmetric cognitive development. Any potential participant manifesting a significant discrepancy between IQ and reading and/or math development also was eliminated owing to the potential of confounds associated with an underlying learning disability. The Devereux Scale for Mental Disorders (Naglieri, LeBuffe, & Pfeiffer, 1994) was used to assess social and emotional development. A t score ≥ 60 on any of the Devereux Scales (conduct, attention, anxiety, depression, autism, acute problems) eliminated a child from the study owing to potential confounds associated with psychopathology. The FH-RDC (Andreasen et al., 1977) interview was given to rule out *Diagnostic and Statistical Manual*, 4th edition (DSM-IV) psychiatric disorders in first-degree relatives. A pediatrician performed a medical examination, including Tanner staging of physical development, for each child at entry into the study to correspond with the MR examination. All tests included in the battery are appropriate for use across the age span of the study, are developmentally sensitive, and have established age norms. The full neurocognitive battery included measures of cognitive domains, divided here into language, visual-spatial construction, executive function, and memory abilities. The specific tests assigned to each domain are listed in Table 1. A composite score was computed for each domain by adding the scores of the tests and dividing by the number of tests used.

A set of test variables from the entire battery was selected to assess the cognitive domains of language, visual spatial, executive function, and memory. The cognitive domain scores were used for determination of associations with selected

https://doi.org/10.1017/S1355617709990233 Published online by Cambridge University Press

Table 1. Neuropsychological test variables used within each cognitive domain

Domain	Test	Variables
Language	Abbreviated WISC for Children	Total Verbal raw scores
	Wechsler Individual Scale of Intelligence (WASI) for Adults	Total Verbal raw scores
	Wechsler Individual Achievement Test (WIAT)	Reading, Spelling raw scores
	Clinical Evaluation of Language Fundamentals (CELF)	Concepts and Directions raw scores
	Peabody Picture Vocabulary Tests	Raw scores
Executive Function	Wechsler Similarities and Matrix Reasoning Subtests	Raw scores
	Wisconsin Card Sorting Test	Perseverative errors
Visual Spatial	Wechsler Block Design	Raw scores
	Visual Motor Integration Test	Raw scores
	Test of Visual Perception	Spatial Relations Subtest raw scores
Memory	Wide Range Assessment of Memory and Learning (WRAML)	Picture Memory, Design Memory, Verbal Learning, Story Memory and Number/Letter Subtests

MRSI variables and GM. The first step was determining which of these cognitive measures, if any, were associated with the three MRSI variables, PCr, sPME/sPDE, and NAA. This analysis was followed by determining if synaptic elimination, represented by GM, was associated with the values of PCr, sPME/sPDE, and NAA. It was predicted that changes in one or more of the molecular indices obtained through the use of curve fitting procedures would coincide with or precede evidence of synaptic development and elimination. Cognitive tests were used to evaluate the overall strength of association among cognitive function, the targeted metabolites, and GM.

Magnetic Resonance Procedures

MRI and MRSI procedures were conducted using a doubly tuned transmit/receive volume head coil on a GE LX 1.5-Tesla whole-body MRI system (GE Medical Systems, Milwaukee, Wisconsin). A 3-dimensional volume of T1-weighted images covering the entire brain (spoiled gradient recalled acquisition [SPGR], repetition time [TR] = 25 ms, echo time [TE] = 5 ms, flip angle = 40°, field of view [FOV] = 24 × 18 cm^2, slice thickness = 0.15 cm, 124 coronal slices, number of excitations [NEX] = 1, matrix = 256 × 192, scan time = 7 min 44 s) was then collected for tissue-segmentation analysis of the ^{31}P spectroscopy voxels. In addition, a set of T2-weighted/proton density images (2-dimensional fast spin-echo, TR = 3,000 ms, echo times = 17 and 102 ms, echo-train length = 8, FOV = 24 × 24 cm^2, approximately 24 axial slices, 5-mm thick and no gap, NEX = 1, matrix = 256 × 192, scan time 5 min 12 s) was used to screen for neuroradiological abnormalities.

^{31}P MRSI acquisition

To prescribe the MRSI slice location, a 3-plane MRI localizer image was first collected, followed by a set of sagittal and axial scout images using the two-dimensional fast spin-echo sequence. Using the mid-sagittal image, the anterior commissure-posterior commissure (AC-PC) line was defined and a 3.0 cm axial slice was positioned parallel to and superior to the AC-PC line for the spectroscopy (Fig. 1A). Prior to the spectroscopy, automatic and manual shimming was applied to the axial slice. A single-slice selective excitation radio frequency (RF) pulse followed by phase-encoding pulses to spatially encode the two dimensions of the slice (termed FIDCSI on a GE system) was used to acquire the multi-voxel *in vivo* ^{31}P spectroscopy data (Fig. 2). The acquisition parameters were: FOV = 24 × 36 cm^2; slice thickness = 3.0 cm; 8 × 8 phase encoding steps (nominal voxel volume = 3.0 × 4.5 × 3.0 cm^3); TR = 2,000 ms; complex data points = 1,024; spectral bandwidth = 5.0 kHz; preacquisition delay = 1.7 ms; number of averages = 16; and acquisition time approximately 34 min.

^{1}H MRSI acquisition

This acquisition method combined the point-resolved spectroscopy sequence (PRESS, [Bottomley, 1987]) with the phase encoding steps of a chemical shift imaging (CSI) sequence, which is termed PRESSCSI, and is part of the GE spectroscopy package. Briefly, the 90° RF pulse followed by two 180° RF pulses, which make up this double-echo sequence, are all slice-selective, and the intersection of the three orthogonal planes defines a large region of interest (ROI). In this study the ROI is positioned in the axial plane, and the left-right and anterior-posterior dimensions will vary accordingly to ensure the ROI covers the brain in the defined axial plane. Surrounding the ROI in the axial plane are four spatially localized saturation slices to suppress the strong lipid signal at the corners of the ROI. Very selective suppression pulses are used for the PRESS localization and the lipid saturation, which provide a much sharper excitation slice profile relative to conventional pulses (Roux, 1998). An example of quantified short TE ^{1}H spectroscopy data, which is collected as described earlier, is shown in Figure 3. Experimental parameters for the water-suppressed PRESSCSI measurement were: FOV = 24 × 24 cm^2; thickness of the

https://doi.org/10.1017/S1355617709990233 Published online by Cambridge University Press

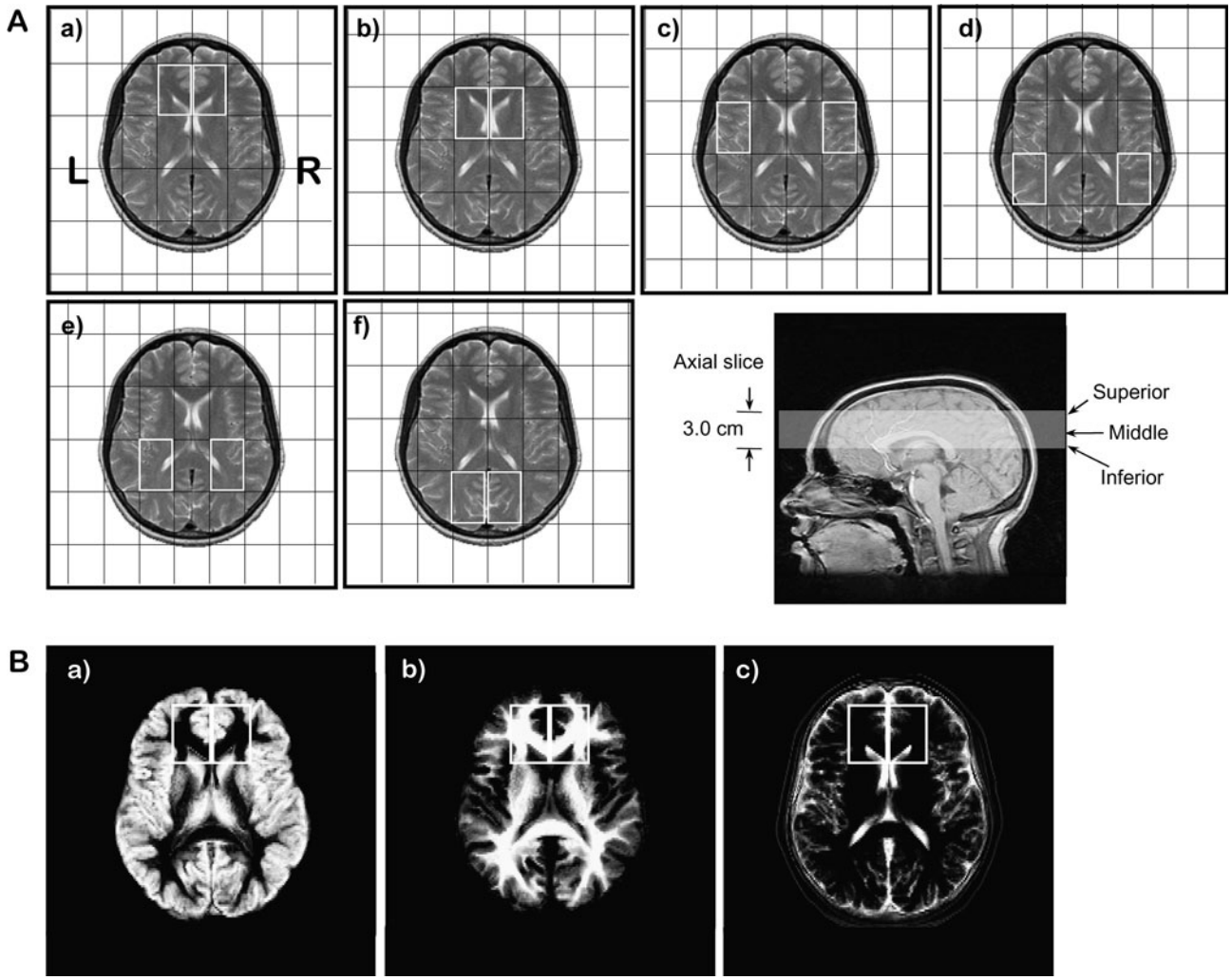

Fig. 1. (A) ^{31}P MRSI voxel grid shifts (outlined in white) superimposed on the middle MRI axial slice (bottom right) for: (a) prefrontal cortex; (b) basal ganglia; (c) superior temporal cortex; (d) inferior parietal cortex; (e) centrum semiovale; and (f) occipital regions. Voxel size is $3.0 \times 4.5 \times 3.0$ cm^3. (B) Segmentation images of: (a) gray matter; (b) white matter; and (c) cerebral spinal fluid (CSF) and extra-cortical matter where the intensity is proportional to the tissue type of that image. Both cortical and subcortical gray matter were measured. The matrix size of the images is 256 in the sagittal direction by 124 in the coronal direction, reflecting the 124 slices that were acquired for the 3-dimensional SPGR sequence. Right and left ^{31}P prefrontal voxels (white boxes) are superimposed on the images.

ROI slice = 2.0 cm; phase encoding steps = 16 × 16 (nominal voxel dimension = 1.5 × 1.5 × 2 cm^3); TR = 1,500 ms; TE = 30 ms; complex data points = 2,048; spectral bandwidth = 2.5 kHz; and NEX = 2. Using identical experimental parameters, water-unsuppressed PRESSCSI data also were collected for post-processing purposes, except there are 8 × 8 phase encoding steps. The ^{1}H MRSI acquisition time is approximately 30 min.

MRSI post-processing and quantification

To minimize the partial volume effect for sampled regions, six different voxel grid shift schemes (Fig. 1A) were applied to both ^{1}H and ^{31}P MRSI prior to 2-dimensional inverse Fourier transformation (2D IFT). These grid schemes provided voxels that include left and right: prefrontal cortex (LPFC, RPFC), superior temporal cortex (LSTC, RSTC), inferior parietal cortex (LIPC, RIPC), basal ganglia (LBG, RBG), and centrum semiovale (LCS, RCS).

Spectral fitting of ^{31}P MRSI

For ^{31}P MRSI, a mild spatial apodization was applied in k-space (Fermi window with 90% diameter and 5% transition width), resulting in an effective voxel size of approximately 46.4 cm^3, whereas a 5 Hz Gaussian apodization is applied in the chemical shift domain and PME, PDE, PCr, α-, β-, and γ-adenosine-5′-triphosphate (ATP), and inorganic orthophosphate (Pi) were modeled in the time domain with Gaussian-damped sinusoids and by omitting the first 4.95 ms of the free induction decay (FID) using the Marquardt-Levenberg algorithm (Fig. 2). This approach ensured that PME and PDE resonances primarily reflected freely mobile short NMR correlation time components (Stanley & Pettegrew,

https://doi.org/10.1017/S1355617709990233 Published online by Cambridge University Press

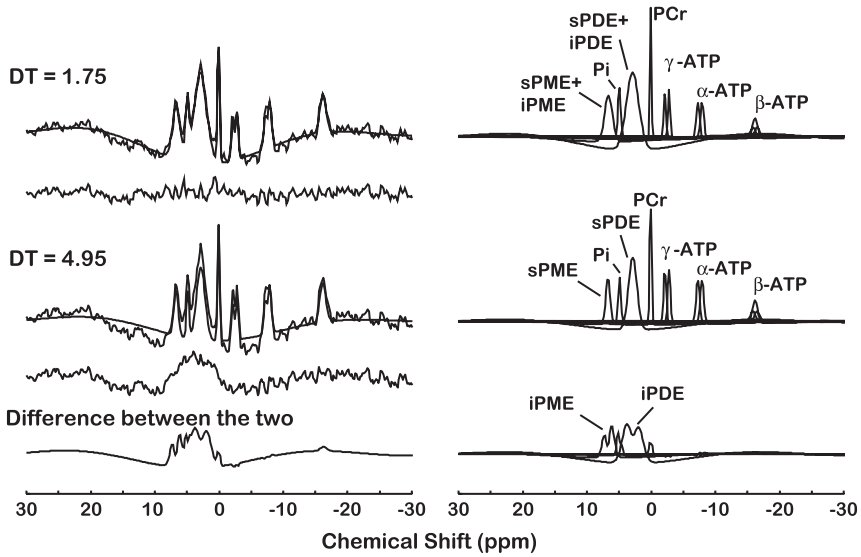

Fig. 2. Quantification of a typical *in vivo* ^{31}P magnetic resonance spectroscopic imaging spectrum with 5 Hz line broadening from a single voxel ($3.0 \times 4.5 \times 3.0$ cm^3) of a study subject. The acquired spectrum is modeled in the time domain with Gaussian-damped sinusoids and by omitting both the first 1.75 ms and first 4.95 ms of the free induction decay using the Marquardt-Levenberg algorithm. Both the short (1.75 ms) and long (4.95 ms) delay time (DT) models are shown superimposed on the acquired ^{31}P spectra, and the modeled resonances are identified on the right. The difference between the two time-domain fits results in the bottom trace containing the intermediate correlation time components.

2001). ^{31}P MRSI quantification was expressed in relative mole percent of the observable ^{31}P resonances. The mole percent method of quantification highly correlates with absolute quantification methods (Klunk, Xu, Panchalingam, McClure, & Pettegrew, 1994).

Spectral fitting of short TE ^{1}H MRSI

The residual of the unsuppressed water signal between 7 ppm and 4.2 ppm was removed by using the (operator-independent) singular value decomposition (SVD)-based fitting algorithm (de Beer & van Ormondt, 1992). The linear combination (LC) Model software package was used to quantify the ^{1}H metabolites, which include: NAA, glutamate, glutamine, *myo*-inositol, trimethylamines (TMA), total creatine (creatine + phosphocreatine; Cr_t), taurine, alanine, aspartate, γ-aminobutyric acid (GABA), glucose, *scyllo*-inositol, N-acetylaspartylglutamate (NAAG), and the macromolecule signals. The key in simplifying the fitting of the complex overlapping resonances was to incorporate *a priori* knowledge into the fitting algorithm (deGraaf & Bovee, 1990; Provencher, 1993; Stanley, Drost, Williamson, & Thompson, 1995). This included *a priori* knowledge of the macromolecule signals as part of the basis of the LC Model (Seeger, Klose, Mader, Grodd, & Nagele, 2003). The LC Model software package, which is commercially available, provided this feature and has been demonstrated by others (Brockmann, Pouwels, Christen, Frahm, & Hanefeld, 1996; Ebert, Speck, Konig, Berger, Hennig, & Hohagen, 1997; Frahm & Hanefeld, 1996) to be an accurate and reliable method to quantify short TE ^{1}H MRS data. The post-processing was fully automated. An example of processed *in vivo* ^{1}H spectrum of a healthy individual using the proposed short TE ^{1}H MRSI technique and the post-processing protocol is shown in Figure 3. Proton MRSI quantification was expressed in mmole.

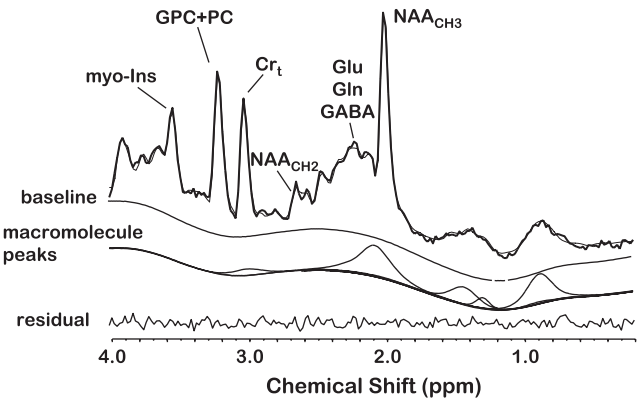

Fig. 3. An example of quantifying a short echo time (TE) ^{1}H MRSI spectrum of a control subject using the proposed acquisition protocol and LC Model fitting. The acquired spectrum with no line broadening is superimposed on the modeled and baseline spine function and the residual is below. The quantified macromolecule signal is indicated in a separate trace.

Morphometry

A fully automated segmentation procedure was used to segment T1- weighted 3D-SPGR images. The functional magnetic resonance imaging of the brain (FMRIB) software Library (FSL; Smith et al., 2004; Woolrich et al., 2009; FSL Analysis Group, FMRIB, Oxford, UK) was used to co-register, correct for any B_1 field bias, brain extraction, and segmentation. The axial slices from the 3D-SPGR images were co-registered

https://doi.org/10.1017/S1355617709990233 Published online by Cambridge University Press

to the axial scout images using FMRIB's linear image registration tool (FLIRT) of the FSL package. The brain extraction tool (BET) software was used to extract brain by removing nonbrain matter from the image. FMRIB's automated segmentation tool (FAST) was used to segment the brain into gray, white, and CSF/extra cortical space while also correcting for spatial intensity variations (also known as bias field or B_1 field inhomogenity correction). Both cortical and subcortical GM were measured. Tools from the software package FreeSurfer (http://surfer.nmr.mgh.harvard.edu) were used to convert the MRI images from ANALYZE format to neuroimaging informatics technology initiative (NIFTI) format, extract header information, and provide intensity normalization prior to segmentation.

Tissue fractions were then calculated by extracting from segmented images the region of interest matching the coordinates and size of ^{31}P spectroscopy voxels using miscellaneous FSL utilities for converting and processing images (FSLUTILS) tools (FSLROI, FSLSTATS, FSLMATHS). A segmented image and voxel placement are illustrated in Figure 1B.

Data analysis

We evaluated subjects across the age range (6–18 years) that covers the physical developmental stages of childhood (6–10 years), pubescence (10–12 years), and adolescence (12–18 years). Molecular and neuromorphometric findings were obtained from 12 brain regions, 6 in each hemisphere. Values for the targeted metabolites were averaged across the axial slice containing the 12 brain regions, thereby yielding a single axial slice value for each metabolite. Our study's primary hypothesis is that neuromolecular underpinnings of synaptic development and elimination, major processes in neurodevelopment, will coincide with or precede changes in GM, and will be observed by differences in the targeted brain metabolites among age groups, accompanied by corresponding differences in cognitive function.

To analyze the effect of age, and therefore neurodevelopment, on the targeted metabolites, scatterplots of age *versus* average axial slice metabolite levels were obtained and fitted with a locally weighted scatterplot smoothing function (LOESS; Cleveland, 1979; Cleveland & Grosse, 1988). The scatterplots show transition points approximating ages of known neurodevelopment stages, that is, childhood (6–10 years), pubescence (10–12 years), and adolescence (12–18 years). To more clearly show these transition points for targeted metabolites and GM, we calculated *Z* scores for each. The *Z* scores for each variable were calculated by subtracting the individual value from mean of the entire dataset of that value, divided by the standard deviation. Based on the findings, it was elected to compare the 6–9.5 and the 12–18 year-old age groups. Comparisons of average metabolite levels between the 6–9.5 and 12–18 year-old age groups were performed using two-sided *t* tests.

The same graphic approach was taken in which *Z* values for PCr, composite cognitive test scores, and GM were plotted by age. This step was taken so that cognitive function and metabolite levels could be compared with changes in cerebral cortical GM, which we hypothesized would show an initial growth reflecting synaptic development, followed by a reduction because of synaptic elimination.

Next, strength of association between cognitive function and metabolite levels with age was examined. For this purpose, linear multiple regression analyses were performed relating composite scores for the major cognitive domains, including language, visual spatial, executive function, and memory, to PCr, sPME/sPDE, and NAA levels, as well as GM. Tests and variables used within each domain are listed in Table 1. Because this is an age-difference study, raw scores of cognitive functions were used rather than age-corrected standard scores.

RESULTS

Reliability of MRSI Measures

Reliability results (relative mole percent of observable phosphorus resonances ± *SD* and the coefficient of variation [CV] in parentheses) for the multi-voxel obtained ^{31}P MRSI metabolites quantification are: sPME, 10.4 ± 2.0 (19%); Pi, 5.4 ± 1.3 (24%); sPDE, 28.5 ± 3.3 (12%); PCr, 11.3 ± 1.4 (13%); αATP, 14.3 ± 2.0 (14%); β–ATP, 16.3 ± 2.1 (13%); and γ–ATP, 13.8 ± 2.6 (19%). Our ^{1}H MRSI studies gave mean absolute levels, relative to the unsuppressed water signal and appropriate correction factors, and CV of the prominent ^{1}H metabolites as: NAA, 7.41 mM (9.4%); Cr_t, 5.36 mM (13.5%); GPC + PC, 1.44 mM (16.8%); *myo*-inositol, 4.18 mM (20.8%); glutamate, 6.53 mM (20.4%); glutamine 2.77 mM (51.8%); and combined macromolecule signal 5.94 (33.4%) (scaled to H_2O resonance, but uncorrected for relaxation times and total number of observable protons). Quantification of the NAA resonance was most reliable (CV = 9.4%); however, measures of glutamate and *myo*-inositol were more variable (CV = 20%) and glutamine was highly variable (CV = 52%). The mean absolute metabolite levels and the variance were consistent with prior short TE studies at 1.5T (Bartha, Drost, Menon, & Williamson, 2000; Brockmann et al., 1996; Ebert et al., 1997; Frahm & Hanefeld, 1996; Kreis, 1997; Provencher, 1993; Stanley et al., 1995). These CV values demonstrate sufficient reliability, enabling us to conduct ^{31}P-^{1}H MRSI studies for the hypotheses to be tested.

MRSI Metabolite Level Changes With Age

Metabolite and GM levels (Fig. 4) and cognitive scores (Fig. 5) were plotted by age using a LOESS smoothing function. These plots demonstrate age-related transition points at 9.5 and 12 years for PCr, sPME/sPDE, and GM. Figure 6 displays the change of PCr, sPME/sPDE ratio, and GM by converting the metabolite levels and GM to *Z* scores. Guided by these plots and other neurodevelopmental data, the metabolite and GM data were grouped into ages 6–9.5, 9.5–12, and 12–18 years old in order to analyze changes in the metabolite levels with age.

https://doi.org/10.1017/S1355617709990233 Published online by Cambridge University Press

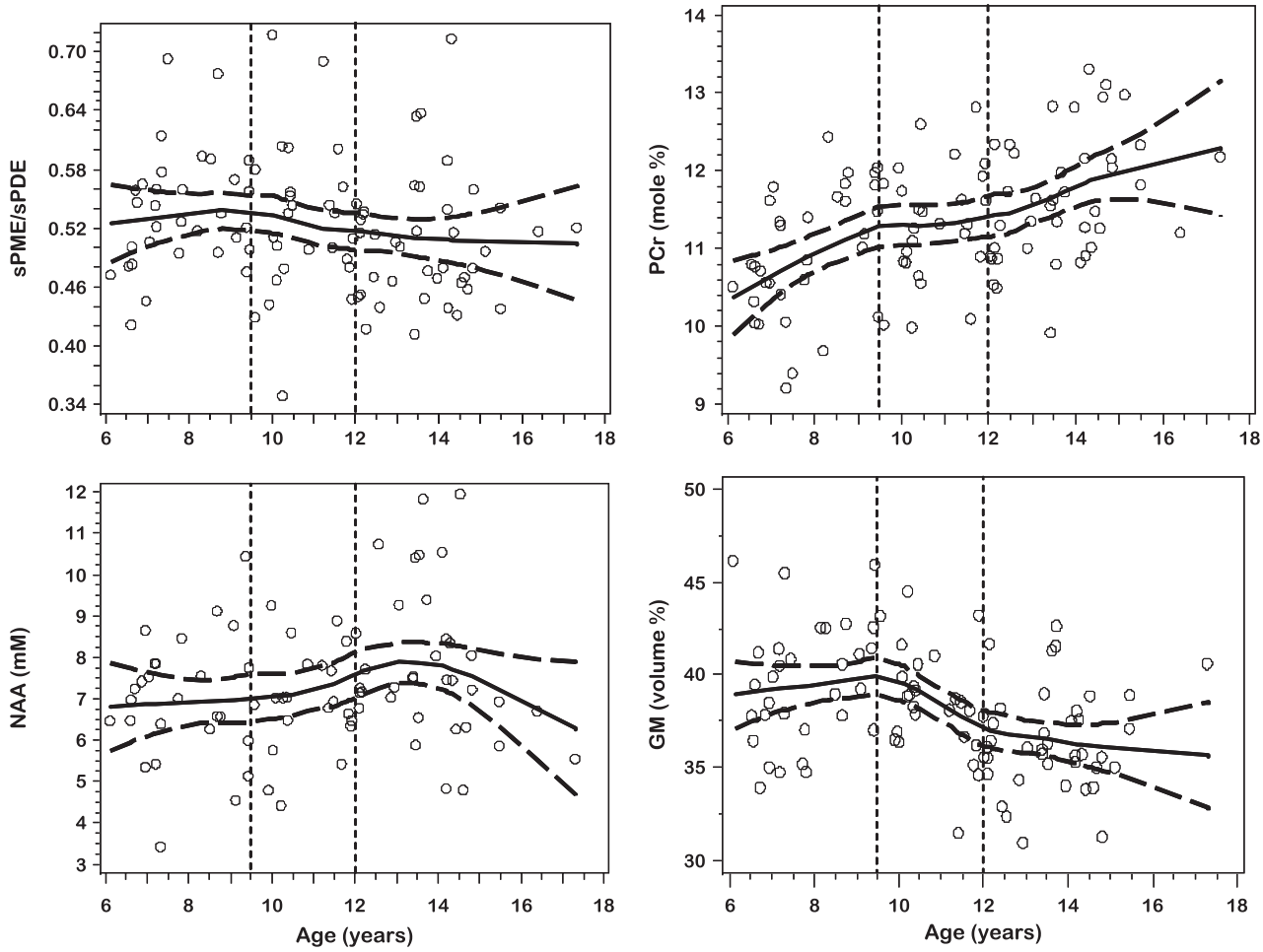

Fig. 4. Scatterplots of PCr, sPME/sPDE, NAA, and GM *versus* age fitted with a LOESS curve with 95% confidence intervals.

Metabolic and GM Differences Among Age Groups

Descriptive statistics for evaluating differences in PCr, sPME/sPDE, GM, and composite cognitive scores among the 6–9.5, 9.5–12, and 12–18 year-old age groups are presented in Table 2. Because there were clear inflections in metabolite levels and GM in the 6–9.5 and 12–18 year-old age groups and a flattening in the 9.5–12 year-old group, we performed the statistical analysis as two group comparisons using two-sided *t* tests. The results indicated that comparing 6–9.5 year-olds to the 12–18 year-olds, PCr was lower in the younger age group (PCr, $p = .0001$), and GM ($p = .0013$) and sPME/sPDE ratio ($p = .046$) were higher. No significant difference was found for NAA comparing the 6–9.5 year-olds with 12–18 year-olds. The CV for PCr (13%) also is much smaller than those for sPME (19%), but similar to those for sPDE (12%) and NAA (9.4%).

Relations Among, PCr Levels, Cognitive Function, and GM With Age

Of the metabolites measured, PCr most directly reflects synaptic activity (see Discussion). For purposes of these graphic analyses, all scores were converted to *Z* scores, allowing for their comparisons on the same scales. Figure 7 illustrates the profiles of various cognitive domains across the age groups placed on the same graphs as PCr and GM. In general, PCr level tracked the cognitive changes quite closely. The rate of PCr increase in the 6–9.5 year-olds is similar to the rate of increase in GM. Within the 9.5 to 12 year age range the slope of PCr is approximately flat, while GM sharply decreases. GM is characterized by an increase in the 6–9.5 year-old age group, and then a marked decrease in the 9.5–12 year-old age group, with virtually no change from 12 to 18 years. PCr continued to increase in the 12 to 18 year-old age range.

Correlations of Composite Cognitive Scores With MRSI Metabolite Levels and GM

Multiple linear regression analysis of composite cognitive scores with average axial slice metabolite levels and GM (Table 3) demonstrated significant correlations of PCr levels and GM with age and language, visual-spatial construction, and memory domains. NAA showed a significant correlation only with the visual-spatial construction domain. These findings

https://doi.org/10.1017/S1355617709990233 Published online by Cambridge University Press

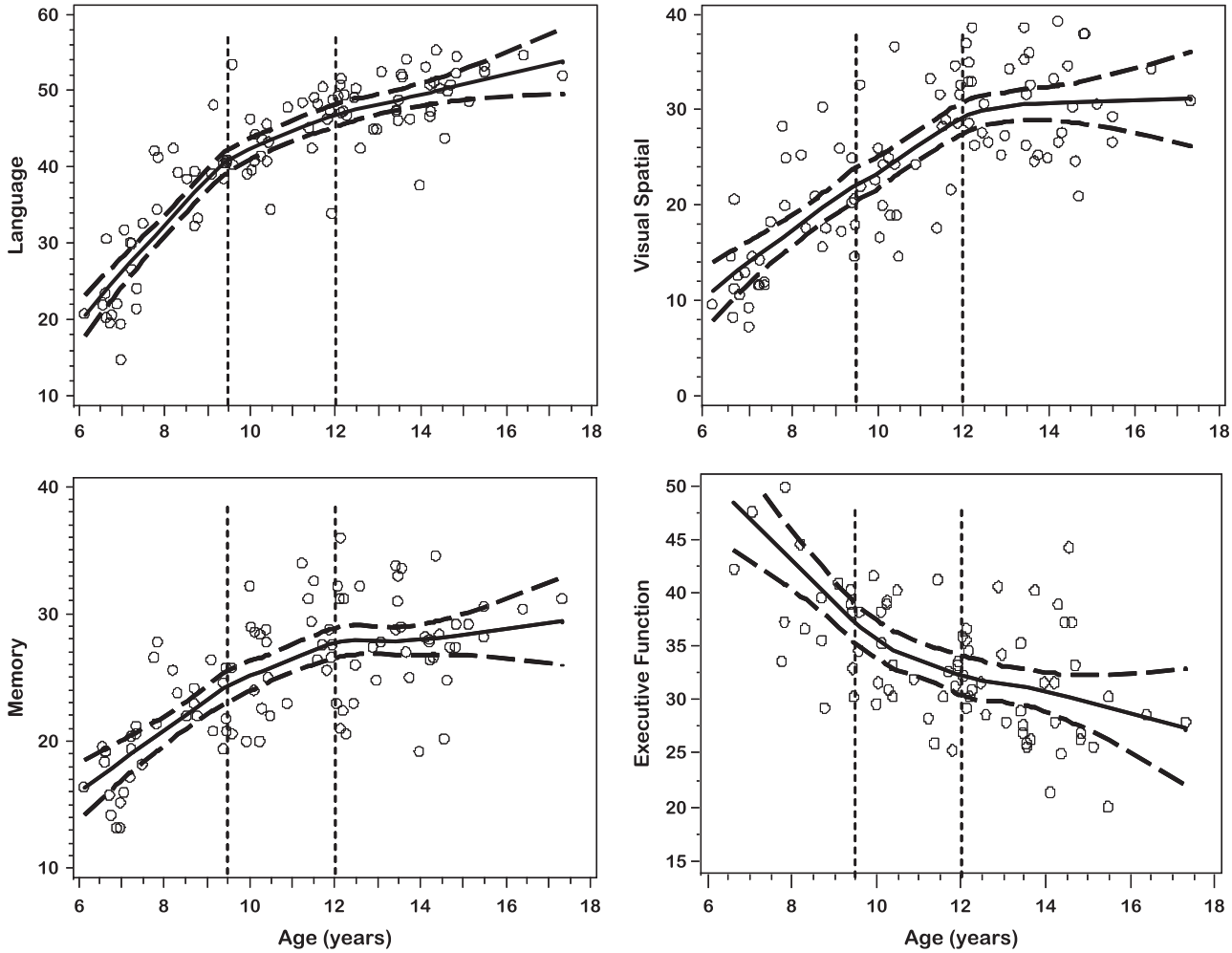

Fig. 5. Scatterplots of composite scores for cognitive domains (Language, Memory, Visual Spatial, Executive Function) *versus* age fitted with a LOESS curve with 95% confidence intervals.

taken together strongly suggest that cognitive function correlates with synaptic activity and not simply with the amount of GM.

DISCUSSION

In this cross-sectional age difference study, we investigated the relationship between a set of ^{31}P-^{1}H MRSI measured metabolites and cognitive development. We did morphological studies for the purpose of evaluating GM across age groups. The major hypothesis was that neuromolecular underpinnings of synaptic development and elimination would reflect age-related cognitive development and coincide or precede change in GM.

The hypothesis would be supported if there were significant correlations in the appropriate direction between the metabolites and cognitive tests of varying abilities. We studied tests of language, visual-spatial construction abilities, executive function, and memory. Multiple correlations were computed to evaluate the strength of association between tests within the domains and the metabolites. In general, there was a significant degree of association between changes in the levels of PCr and age-associated improvement in cognitive ability, but not with GM.

Table 2. Descriptive statistics of axial slice MRSI metabolites and GM by age group

	6–9.5 (years)			9.5–12 (years)			12–18 (years)			6–9.5 *vs.* 12–18
Age group	*M*	*SD*	*n*	*M*	*SD*	*n*	*M*	*SD*	*n*	*p*
sPME/sPDE	0.538	0.059	33	0.528	0.078	26	0.507	0.063	40	.046
PCr (mole %)	10.95	0.82	33	11.33	0.74	26	11.66	0.81	40	.0001
NAA (mM)	6.98	1.52	26	6.98	1.26	21	7.82	1.82	35	not significant
GM (volume %)	39.88	3.45	26	38.65	38.65	25	36.31	2.94	40	.0013

https://doi.org/10.1017/S1355617709990233 Published online by Cambridge University Press

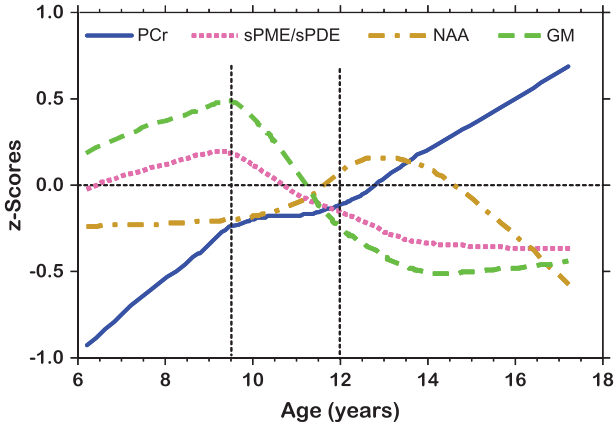

Fig. 6. *Z* score plots of PCr, sPME/sPDE, NAA, and GM *versus* age.

NAA Levels

NAA (470–974 μmoles/100 g; McIlwain & Bachelard, 1985, p. 155), which is second to glutamate (781–1250 μmoles/100 g; McIlwain & Bachelard, 1985, p. 155) in terms of total brain concentration of free amino acids, accounts for approximately 85–90% of the proton signal of the N-acetyl methyl group, and NAAG contributes to the remaining 10–15% (Frahm, Michaelis, Merboldt, Hanicke, Gyngell, & Bruhn, 1991; Koller, Zaczek, & Coyle, 1984; Pouwels & Frahm, 1997). Both NAA and NAAG are localized exclusively in mature neurons and neuronal processes, and not in mature glia (Birken & Oldendorf, 1989; Koller et al., 1984; Tallan, Moore, & Stein, 1956; Urenjak, Williams, Gadian, & Noble, 1993). NAA is formed in mitochondria from acetyl-CoA and aspartate by the membrane bound enzyme L-aspartate N-acetyltransferase, an enzyme found in brain but not in other tissue, such as heart, liver, and kidney (Goldstein, 1959, 1969; Knizley, 1967; Truckenmiller, Namboodiri, Brownstein, & Neale, 1985). Monoclonal antibody studies show NAA to be localized to neurons with intense staining of the perikarya and proximal dendrites and axons (Simmons, Frondoza, & Coyle, 1991). The neuronal immunoreactivity does not correspond to primary neurotransmitter characteristics. A recent report of whole brain NAA levels in young adults gave a value of 9.5 ± 1.0 mM in white matter and 14.3 ± 1.1 mM in gray matter (Inglese, Rusinek, George, Babb, Grossman, & Gonen, 2008).

N-Acetyl moieties with short correlation times, such as found in N-acetyl-sugars (N-acetyl-galactosamine, N-acetyl-glucosamine, N-acetyl-neuraminic acid), and glycosphingolipids, such as gangliosides, also can contribute to the "NAA" resonance. Gangliosides are enriched in gray matter (Agranoff

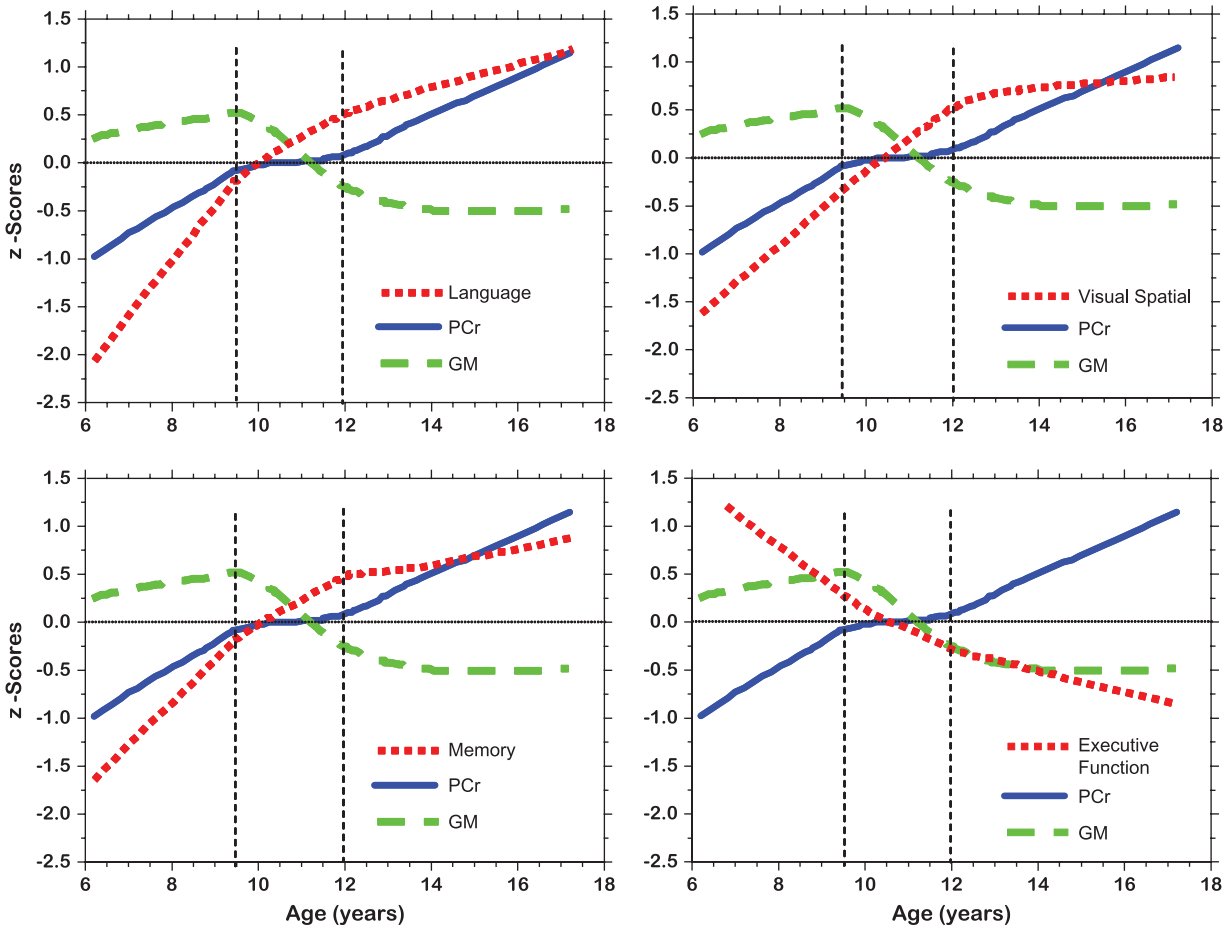

Fig. 7. *Z* score plots of PCr, GM, and cognitive domain composite scores (Language, Memory, Visual Spatial, Executive Function).

https://doi.org/10.1017/S1355617709990233 Published online by Cambridge University Press

Table 3. Multiple linear regression analysis relating composite scores for cognitive domains with MRSI metabolite levels and GM

	Age		Language		Visual Spatial		Executive Function		Memory	
	r	*n*	*r*	*n*	*r*	*n*	*r*	*n*	*r*	*n*
PCr	.474***	99	.421***	96	.234*	94	.076	79	.291**	98
sPME/sPDE	–.150	98	–.064	95	–.108	94	.008	79	.009	97
NAA	.208	85	.173	83	.237*	81	.135	69	.159	85
GM	–.399***	81	–.287*	78	–.368***	76	–.223	69	–.323**	80

Note. PCr = phosphocreatine; sPME/sPDE = short NMR correlation time phosphomonoester/phosphodiester ratio; NAA = N-acetylaspartate; GM = percent gray matter by volume.
***$p \leq .001$; **$p \leq .01$; *$p \leq .05$ (2-tailed); *r* is the Pearson correlation.

& Hajra, 1994), where they are enriched in synaptic membranes (Whittaker, 1966; Wiegandt, 1967). The levels of gangliosides in human brain cerebral gray matter (1.45–1.68 mmoles/100 g dry weight) and cerebral white matter (0.28–0.37 mmoles/100 g dry weight) have been determined by Eeg-Olofsson, Kristensson, Sourander, & Svennerholm, (1966). The levels of gangliosides are developmentally regulated (Suzuki, 1966). Sialoproteins also contain N-acetylneuraminic acid and could contribute up to 15% of the total brain protein (McIlwain & Bachelard, 1985, p. 316).

sPME/sPDE Ratio

The sPME/sPDE ratio reflects metabolite turnover of membrane phospholipids, such as phosphatidylcholine, phosphatidylethanolamine, and phosphatidylserine. With net synthesis of these phospholipids sPME/sPDE is greater than 1, with net breakdown it is less than 1, and equals 1 when synthesis and breakdown are in equilibrium. Increased sPME are found at the site and time of neuritic sprouting in brain and sPDE are increased at the site and time of membrane breakdown (Geddes, Panchalingam, Keller, & Pettegrew, 1997). sPME and sPDE are not involved in the synthesis or breakdown of glycosphingolipids, such as gangliosides, which are enriched in synaptic membranes (Whittaker, 1966; Wiegandt, 1967). sPME/sPDE increases from age 6 to 9.5 years reflecting active synthesis of membrane phospholipids, followed by decreases until approximately 14 years of age, with evidence for net phospholipid breakdown from age 11 to 14 years. The GM curve also is shown in Figure 6. As observed, GM increases for ages 6 to 9.5 years followed by a steeper decline until approximately 13 years. Changes in GM were consistent with synaptic development, followed by synaptic elimination, and are in keeping with the neuromorphometric findings of Giedd et al. (1999) and Gogtay et al. (2007), the molecular findings of Geddes et al. (1997), and the histological data of Huttenlocher and Dabholkar (1997). Note that the rate of increase in GM from 6 to 9.5 years and decrease from 9.5 to 13 years is greater than for sPME/sPDE. The difference in these rates (GM *vs.* sPME/sPDE) could be a result of ganglioside contributions to the gray matter.

Phosphocreatine

Brain tissue contains approximately 3 $\mu mole \cdot g^{-1}$ ATP, which could maximally provide 6 $\mu moles \cdot g^{-1}$ of high-energy phosphate. ATP utilization in rat brain is approximately 0.5 $\mu moles \cdot g^{-1}\ s^{-1}$ and therefore available stores of ATP would last approximately 12 s without new ATP production (Siesjo, 1978, p. 12). However, PCr is a storage form of ATP that can be converted to ATP by the creatine kinase (CrK) enzyme according to the reaction:

$$PCr + ADP + H^{+} \underset{E.C.2.7.3.2}{\overset{CrK}{\rightleftharpoons}} Cr + ATP$$

This is an equilibrium reaction ($\Delta G = 0$), that is, no net flux in either direction. ATP synthesis is stimulated by a reduction in ATP or increases in ADP or $[H^+]$. In a comprehensive review, Andres, Ducray, Schlattner, Wallimann, & Widmer, (2008) describe PCr as a spatial energy "shuttle" or "circuit" that bridges sites of ATP generation and consumption. Brain concentration of PCr is approximately 5 $\mu mole\ g^{-1}$ and therefore the stores of high-energy phosphate (ATP + PCr) will be consumed after about 20 s of continuous utilization (Siesjo, 1978, p. 12). Several studies have shown that anesthesia causes an elevation of PCr and ATP in parallel to the decrease in neuronal activity (Hein, Krieglstein, & Stock, 1975; McCandless & Wiggins, 1981). Sokoloff (1991, 1993) also has shown that the synapse is the site of highest energy consumption during increased activity and that most of this consumption is in the recovery period, rather than during the activity itself. This is consistent with the studies of Jansson, Harkonen, & Helve, (1979) who showed that PCr and ATP levels are lower in isolated cerebral nerve endings than in whole brain. Unlike nerve tissue in general, synaptosomes preferentially utilize endogenous PCr and ATP stores. Jansson et al. (1979) concluded that synaptic transmission primarily depends on local stores of high-energy phosphates, rather than on the availability of glucose per se. Results of human ^{31}P fMRS monitoring of brain PCr levels before, during, and following visual cortical activation are in keeping with the presented explanations (Rango, Castelli, & Scarlato, 1997; Rango, Bozzali, Prelle, Scarlato, & Bresolin, 2001).

https://doi.org/10.1017/S1355617709990233 Published online by Cambridge University Press

Other sources of ATP production, such as oxidative phosphorylation and glycolysis, come into play after the consumption of PCr pools.

PCr levels are low at age 6 and then sharply increase until age 10. From age 10 to 12 years the increase in PCr levels is much less, but from age 12 to 17 years PCr levels again sharply increase. The low levels of PCr at age 6 years are consistent with the active synthesis of membrane phospholipids, which require ATP. For example, one mole of dipalmitoylphosphatidylcholine (DPPC) derived from *de novo* synthesis requires 295 moles of ATP. The breakdown of DPPC recovers only 258 moles of ATP from the oxidation of both palmitates. Therefore, the complete synthesis and breakdown of 1 mole of DPPC results in an energetic debt of 37 moles of ATP. The acylation/deacylation of DPPC results in an energetic debt of 2 moles of ATP. Likewise, the *de novo* synthesis of 1 mole of cholesterol, a major membrane constituent, requires 276 moles of ATP, with no ATP recovered from the breakdown of cholesterol (Pettegrew, Keshavan, Stanley, McClure, Johnson, & Panchalingam, 2003).

The slow increase in PCr levels from ages 9.5 to12 years coincides with a steep decrease in GM and a less rapid decrease in the sPME/sPDE ratio. One might speculate that the membranes being lost are predominantly nonphosphorus-containing glycosphingolipids, such as gangliosides, which are predominantly found in gray matter and are enriched in synaptic membranes. By this reasoning, the decrease in GM is most likely a result of the decrease in synaptic membranes contained in the neuropil.

The decline in GM from 12 to 18 years corresponds to continued increases in PCr. In the brain, ATP is primarily consumed at synaptic membranes for repolarizing synaptic membranes, which have been depolarized, and PCr is the buffer for ATP (Buchli, Martin, Boesiger, & Rumpel, 1994; Chugani, Phelps, & Mazziotta, 1987; Frey, 1994; Hein et al., 1975; Hess, 1961; Jansson et al., 1979; Kadekaro, Crane, & Sokoloff, 1985; Kennedy & Sokoloff, 1957; McCandless & Wiggins, 1981; Sokoloff, 1966, 1991). The increase in PCr in the 12–18 year-olds could be caused by synaptic elimination, resulting in fewer synapses or decreased activity of remaining synapses in older subjects.

Correlations Among PCr Levels, GM, and Cognitive Composite Scores

Both PCr and GM in the axial slice are highly correlated with age, but NAA, sPME, sPDE, and sPME/sPDE are not. In addition, both PCr and GM in the axial slice are correlated with language, visual-spatial construction, and memory, but not with executive function. Finally, PCr levels and GM in the axial slice correlate ($r=-.304$; $p=.0026$) with each other, but NAA and GM are not correlated ($r=-.023$; $p=.835$). These findings taken together and inspection of Figure 6 suggest that axial slice PCr levels, in general, follow a curve similar to curves for the various cognitive domains. However, the curve for GM has qualitative findings dissimilar to the curve for PCr, which is consistent with synaptic elimination (GM curve) and the functional consequence of synaptic elimination or reduced synaptic activity (PCr curve). Finally, given the lack of correlation between NAA and GM, it may be that there are other molecular contributions to the "NAA" resonance signal besides N-acetylaspartate, as discussed earlier.

CONCLUSIONS

Our data demonstrate neurodevelopmentally determined changes in cognition (executive, language, memory, visual-spatial), and brain molecular composition (PCr, sPME/sPDE, NAA), and structure (GM) in humans ages 6–18 years. sPME/sPDE and GM changes coincide and likely reflect synaptogenesis (6–9.5 years), followed by synaptic elimination in gray matter neuropil (9.5–12 years). Neurodevelopmental changes in PCr support this explanation and reflect PCr utilization for both membrane phospholipid synthesis and synaptic repolarization from 6–9.5 years (synaptogenesis), followed by synaptic elimination (ages 9.5–12 years), resulting in reduced PCr utilization for both membrane phospholipid synthesis and synaptic repolarization (12–18 years). PCr levels and GM highly correlate with each other and with acquisition of cognitive abilities across several cognitive domains. This suggests that neuropil synaptic numbers and activity correlate with cognitive development and not simply with the GM. Of interest, is the observation that neurodevelopmental changes in NAA levels occur later than those related to synaptic numbers and function (Fig. 6). Because NAA is considered a marker of neuronal perikaryon and axons, the lack of NAA correlation with age or cognitive domain composite test scores (except visual-spatial, $p \leq .05$) suggests there could be other molecular contributors to the "NAA" signal besides N-acetylaspartate.

This study has several limitations. The data are based on cross-sectional analysis, though it is not likely the cross-sectional data were markedly influenced by cohort effects, because all subjects were recruited from the same community over a period of only four years. There is the possibility of gender differences, which we could not evaluate because of small sample sizes. A final consideration is that the data was obtained from an axial slice of brain and different results may be found at different regional locations.

ACKNOWLEDGMENTS

This work was supported in part by an NIHCD/NIH HD-39799 grant (JWP). We thank Terry Bradbury for conducting neuropsychological testing. Indebtedness is also expressed to the Medical Research Service and the VISN-IV Mental Illness, Research, Education, and Clinical Center (MIRECC), Department of Veterans Affairs, for support of this work. We thank Harriet Marshman, Deborah Wetzler, and Dennis McKeag for help in conducting the study. There is no conflict of interest on the part of any of the authors.

REFERENCES

Agranoff, B.W., & Hajra, A.K. (1994). Lipids. In G.J. Siegel, B.W. Agranoff, R.W. Albers, & P.B. Molinoff (Eds.), *Basic neurochemistry: Molecular, cellular, and medical aspects* (5th ed., pp. 97–116). New York: Raven Press.

https://doi.org/10.1017/S1355617709990233 Published online by Cambridge University Press

Andreasen, N.C., Endicott, J., Spitzer, R.L., & Winoker, G. (1977). The reliability and validity of the family history method using family history research diagnostic criteria (FH-RDC). *Archives of General Psychiatry*, *34*, 1229–1235.

Andres, R.H., Ducray, A.D., Schlattner, U., Wallimann, T., & Widmer, H.R. (2008). Functions and effects of creatine in the central nervous system. *Brain Research Bulletin*, *76*, 329–343.

Bartha, R., Drost, D.J., Menon, R.S., & Williamson, P.C. (2000). Comparison of the quantification precision of human short echo time (1)H spectroscopy at 1.5 and 4.0 Tesla. *Magnetic Resonance in Medicine*, *44*, 185–192.

Birch, H.G., & Gussow, J.D. (1970). *Disadvantaged children, health, and nutrition and school failure*. New York: Harcourt, Brace & World.

Birken, D.L., & Oldendorf, W.H. (1989). N-Acetyl-L-aspartic acid: A literature review of a compound prominent in ^{1}H-NMR spectroscopic studies of brain. *Neuroscience and Biobehavioral Reviews*, *13*, 23–31.

Bottomley, P.A. (1987). Spatial localization in NMR spectroscopy *in vivo*. *Annals of the New York Academy of Sciences*, *508*, 333–348.

Bourgeois, J.-P. & Rakic, P. (1993). Changes of synaptic density in the primary visual cortex of the Macaque monkey from fetal to adult stage. *Journal of Neuroscience*, *13*, 2801–2820.

Brockmann, K., Pouwels, P.J., Christen, H.J., Frahm, J., & Hanefeld, F. (1996). Localized proton magnetic resonance spectroscopy of cerebral metabolic disturbances in children with neuronal ceroid lipofuscinosis. *Neuropediatrics*, *27*, 242–248.

Buchli, R., Martin, E., Boesiger, P., & Rumpel, H. (1994). Developmental changes of phosphorus metabolite concentrations in the human brain: A ^{31}P magnetic resonance spectroscopy study *in vivo*. *Pediatric Research*, *35*, 431–435.

Chugani, H.R., Phelps, M.E., & Mazziotta, J.C. (1987). Positron emission tomography study of human brain functional development. *Annals of Neurology*, *322*, 487–497.

Cleveland, W.S. (1979). Robust locally-weighted regression and smoothing scatterplots. *Journal of the American Statistical Association*, *74*, 829–836.

Cleveland, W.S., & Grosse, E. (1988). Regression by local fitting. *Journal of Econometrics*, *37*, 87–114.

de Beer, R., & van Ormondt, D. (1992). Analysis of NMR data using time domain fitting procedures. In P. Diehl & E.G. Fluck (Eds.), *NMR basics, principles and progress* (pp. 201–258). New York: Springer-Verlag.

deGraaf, A.A., & Bovee, W.M.M.J. (1990). Improved quantification of *in vivo* ^{1}H NMR spectra by optimization of signal acquisition and processing and by incorporation of prior knowledge into the spectral fitting. *Magnetic Resonance in Medicine*, *15*, 305–319.

Ebert, D., Speck, O., Konig, A., Berger, M., Hennig, J., & Hohagen, F. (1997). 1H-magnetic resonance spectroscopy in obsessive-compulsive disorder: Evidence for neuronal loss in the cingulate gyrus and the right striatum. *Psychiatry Research*, *74*, 173–176.

Eeg-Olofsson, O., Kristensson, K., Sourander, P., & Svennerholm, L. (1966). Tay-Sach's Disease. A generalized metabolic disorder. *Acta Paediatrica Scandinavica*, *55*, 546–562.

Frahm, J., & Hanefeld, F. (1996). Localized proton magnetic resonance spectroscopy of cerebral metabolites. *Neuropediatrics*, *27*, 64–69.

Frahm, J., Michaelis, T., Merboldt, K.D., Hanicke, W., Gyngell, M.L., & Bruhn, H. (1991). On the N-acetyl methyl resonance in localized ^{1}H NMR spectra of human brain *in vivo*. *Nuclear Magnetic Resonance in Biomedicine*, *4*, 201–204.

Frey, K.A. (1994). Positron emission tomography. In G.J. Siegel, B.W. Agranoff, R.W. Albers, & P.B. Molinoff (Eds.), *Basic neurochemistry: Molecular, cellular and medical Aspects* (5th ed., pp. 935–955). New York: Raven Press.

Geddes, J.W., Panchalingam, K., Keller, J.N., & Pettegrew, J.W. (1997). Elevated phosphocholine and phosphatidyl choline following rat entorhinal cortex lesions. *Neurobiology of Aging*, *18*, 305–308.

Giedd, J.N., Blumenthal, J., Jeffries, N.O., Castellanos, F.X., Liu, H., Zijdenbos, A., Paus, T., Evans, A.C., & Rapoport, J.L. (1999). Brain development during childhood and adolescence: A longitudinal MRI study. *Nature Reviews Neuroscience*, *2*, 861–863.

Gogtay, N., Ordonez, A., Herman, D.H., Hayashi, K.M., Greenstein, D., Vaituzis, C., Lenane, M., Clasen, L., Sharp, W., Giedd, J.N., Jung, D., Nugent, T.F., III, Toga, A.W., Leibenluft, E., Thompson, P.M., & Rapoport, J.L. (2007). Dynamic mapping of cortical development before and after the onset of pediatric bipolar illness. *Journal of Child Psychology & Psychiatry & Allied Disciplines*, *48*, 852–862.

Goldstein, F.B. (1959). Biosynthesis of N-acetyl-L-aspartic acid. *Journal of Biological Chemistry*, *234*, 2702–2706.

Goldstein, F.B. (1969). The enzymatic synthesis of N-acetyl-L-aspartic acid by subcellular preparations. *Journal of Biological Chemistry*, *244*, 4257–4260.

Hein, H., Krieglstein, J., & Stock, R. (1975). The effects of increased glucose supply and thiopental anesthesia on energy metabolism of the isolated perfused rat brain. *Naunyn Schmiedebergs Archives of Pharmacology*, *289*, 399–407.

Hess, H. (1961). The rates of respiration of neurons and neuroglia in human cerebrum. In S.S. Kety & J. Elkes (Eds.), *Regional neurochemistry* (pp. 200–202). Oxford, UK: Pergamon Press.

Huttenlocher, P.R. (1979). Synaptic density in human frontal cortex: Developmental changes and effects of aging. *Brain Research*, *163*, 195–205.

Huttenlocher, P.R. (1990). Morphometric study of human cerebral cortex development. *Neuropsychologia*, *28*, 517–527.

Huttenlocher, P.R. & Dabholkar, A.S. (1997). Regional differences in synaptogenesis in human cerebral cortex. *Journal of Comparative Neurology*, *387*, 167–178.

Huttenlocher, P.R., de Courtten, C., Garey, L.J., & Van der Loos, L.H. (1982). Synaptogenesis in human visual cortex: Evidence for synapse elimination during normal development. *Neuroscience Letters*, *33*, 247–252.

Inglese, M., Rusinek, H., George, I.C., Babb, J.S., Grossman, R.I., & Gonen, O. (2008). Global average gray and white matter N-acetylaspartate concentration in the human brain. *Neuroimage*, *41*, 270–276.

Jansson, S.E., Harkonen, M.H., & Helve, H. (1979). Metabolic properties of nerve endings isolated from rat brain. *Acta Physiologica Scandinavica*, *107*, 205–212.

Kadekaro, M., Crane, A.M., & Sokoloff, L. (1985). Differential effects of electrical stimulation of sciatic nerve on metabolic activity in spinal cord and dorsal root ganglion in the rat. *Proceedings of the National Academy of Sciences of the United States of America*, *82*, 6010–6013.

Kennedy, C., & Sokoloff, L. (1957). An adaptation of the nitrous oxide method to the study of the cerebral circulation in children: Normal values for cerebral blood flow and cerebral metabolic rate in childhood. *Journal of Clinical Investigation*, *36*, 1130–1137.

Klunk, W.E., Xu, C.J., Panchalingam, K., McClure, R.J., & Pettegrew, J.W. (1994). Analysis of magnetic resonance spectra by

mole percent: Comparison to absolute units. *Neurobiology of Aging*, *15*, 133–140.

Knizley, H. (1967). The enzymatic synthesis of N-acetyl-L-aspartic acid by a water-insoluble preparation of a cat brain acetone powder. *Journal of Biological Chemistry*, *242*, 4619–4622.

Koller, K.J., Zaczek, R., & Coyle, J. (1984). N-acetyl-aspartyl-glutamate: Regional levels in rat brain and the effects of brain lesions as determined by a new HPLC method. *Journal of Neurochemistry*, *43*, 1136–1142.

Kreis, R. (1997). Quantitative localized ^{1}H MR spectroscopy for clinical use. *Journal of Progress in Nuclear Magnetic Resonance*, *31*, 155–195.

McCandless, D.W., & Wiggins, R.C. (1981). Cerebral energy metabolism during the onset and recovery from halothane anesthesia. *Neurochemical Research*, *6*, 1319–1326.

McIlwain, H., & Bachelard, H.S. (1985). *Biochemistry and the Central Nervous System* (5th ed.). Edinburgh, UK: Churchill Livingstone.

Naglieri, J.A., LeBuffe, P.A., & Pfeiffer, S.I. (1994). *Devereux Scale for Mental Disorders*. San Antonio, TX: Psychological Corporation.

Pettegrew, J.W., Keshavan, M.S., Stanley, J.A., McClure, R.J., Johnson, C.R., & Panchalingam, K. (2003). Magnetic resonance spectroscopy in the assessment of phospholipid metabolism in schizophrenia and other psychiatric disorders. In M. Peet, I. Glen, & D.F. Horrobin (Eds.), *Phospholipid spectrum disorder in psychiatry* (2nd ed., pp. 239–255). Carnforth, UK: Marius.

Pouwels, P.J., & Frahm, J. (1997). Differential distribution of NAA and NAAG in human brain as determined by quantitative localized proton MRS. *Nuclear Magnetic Resonance in Biomedicine*, *10*, 73–78.

Provencher, S.W. (1993). Estimation of metabolite concentrations from localized *in vivo* proton NMR spectra. *Magnetic Resonance in Medicine*, *30*, 672–679.

Rakic, P., Bourgeois, J.-P., Eckenhoff, M.F., Zecevic, N., & Goldman-Rakic, P.S. (1986). Concurrent overproduction of synapses in diverse regions of the primate cerebral cortex. *Science*, *232*, 232–235.

Rango, M., Bozzali, M., Prelle, A., Scarlato, G., & Bresolin, N. (2001). Brain activation in normal subjects and in patients affected by mitochondrial disease without clinical central nervous system involvement: A phosphorus magnetic resonance spectroscopy study. *Journal of Cerebral Blood Flow & Metabolism*, *21*, 85–91.

Rango, M., Castelli, A., & Scarlato, G. (1997). Energetics of 3.5 s neural activation in humans: A ^{31}P MR spectroscopy study. *Magnetic Resonance in Medicine*, *38*, 878–883.

Roux, L. (1998). Magnetic resonance. *Journal of Magnetic Resonance Imaging*, *8*, 1022–1023.

Seeger, U., Klose, U., Mader, I., Grodd, W., & Nagele, T. (2003). Parameterized evaluation of macromolecules and lipids in proton MR spectroscopy of brain diseases. *Magnetic Resonance in Medicine*, *49*, 19–28.

Siesjo, B.K. (1978). *Brain energy metabolism*. New York: Wiley.

Simmons, M.L., Frondoza, C.G., & Coyle, J.T. (1991). Immunocytochemical localization of N-acetyl-aspartate with monoclonal antibodies. *Neuroscience*, *45*, 37–45.

Smiley, J.F., & Goldman-Rakic, P.S. (1993). Heterogeneous targets of dopamine synapses in monkey prefrontal cortex demonstrated by serial section electron microscopy: A laminar analysis using the silver enhanced diaminobenzidine-sulfide (SEDS) immunolabeling technique. *Cerebral Cortex*, *3*, 223–238.

Smith, S.M., Jenkinson, M., Woolrich, M.W., Beckmann, C.F., Behrens, T.E.J., Johansen-Berg, H., Bannister, P.R., De Luca, M., Drobnjak, I., Flitney, D.E., Niazy, R., Saunders, J., Vickers, J., Zhang, Y., De Stefano, N., Brady, J.M., & Matthews, P.M. (2004). Advances in functional and structural MR image analysis and implementation as FSL. *Neuroimage*, *23*(Suppl. 1), 208–219.

Sokoloff, L. (1966). Cerebral circulatory and metabolic changes associated with aging. *Research Publications – Association for Research in Nervous and Mental Disease*, *41*, 237–254.

Sokoloff, L. (1991). Measurement of local cerebral glucose utilization and its relation to local functional activity in the brain. *Advances in Experimental Medicine & Biology*, *291*, 21–42.

Sokoloff, L. (1993). Function-related changes in energy metabolism in the nervous system: Localization and mechanisms. *Keio Journal of Medicine*, *42*, 95–103.

Stanley, J.A., Drost, D.J., Williamson, P.C., & Thompson, R.T. (1995). The use of *a priori* knowledge to quantify short echo *in vivo* ^{1}H MR spectra. *Magnetic Resonance in Medicine*, *34*, 17–24.

Stanley, J.A., & Pettegrew, J.W. (2001). Post-processing method to segregate and quantify the broad components underlying the phosphodiester spectral region of *in vivo* ^{31}P brain spectra. *Magnetic Resonance in Medicine*, *45*, 390–396.

Storm-Mathisen, J., & Otterson, O.P. (1990). Immunocytochemistry of glutamate at the synaptic level. *Journal of Histochemistry and Cytochemistry*, *38*, 1733–1743.

Suzuki, K. (1966). The pattern of mammalian brain gangliosides III. Regional and developmental differences. *Journal of Neurochemistry*, *12*, 969–979.

Tallan, H.H., Moore, S., & Stein, W.H. (1956). N-acetyl-L-aspartic acid in brain. *Journal of Biological Chemistry*, *219*, 257–264.

Truckenmiller, M.E., Namboodiri, M.A.A., Brownstein, M.J., & Neale, J.H. (1985). N-Acetylation of L-aspartate in the nervous system: Differential distribution of a specific enzyme. *Journal of Neurochemistry*, *45*, 1658–1662.

Urenjak, J., Williams, S.R., Gadian, D.G., & Noble, M. (1993). Proton nuclear magnetic resonance spectroscopy unambiguously identifies different neural cell types. *Journal of Neuroscience*, *13*, 981–989.

Volpe, J.J. (1995). Neuronal proliferation, migration, organization, and myelination. In *Neurology of the newborn* (3rd ed., pp. 43–92). Philadelphia: W.B. Saunders.

Wechsler, D. (1974). *Wechsler Intelligence Scale for Children-Revised manual*. New York: Psychological Corporation.

Wechsler, D. (1999). *WASI: Wechsler Abbreviated Scale of Intelligence manual*. San Antonio, TX: Psychological Corporation.

Wechsler, D. (2001). *Wechsler Individual Achievement Test* (2nd ed.), San Antonio, TX: Psychological Corporation.

Whittaker, V.P. (1966). Some properties of synaptic membranes isolated from the central nervous system. *Annals of the New York Academy of Sciences*, *137*, 982–998.

Wiegandt, H. (1967). The subcellular localization of gangliosides in the brain. *Journal of Neurochemistry*, *14*, 671–674.

Woolrich, M.W., Jbabdi, S., Patenaude, B., Chappell, M., Makni, S., Behrens, T., Beckmann, C., Jenkinson, M., & Smith, S.M. (2009). Bayesian analysis of neuroimaging data in FSL. *Neuroimage*, *45*(Suppl. 1), S173–S186.